Microelectronics Reliability 83 (2018) 119–126

Contents lists available at ScienceDirect

Microelectronics Reliability

journal homepage: www.elsevier.com/locate/microrel

First principles calculations study of crystallographic orientation effects on SiC/Ti and SiC/Cr interfaces

Lei Li[a,1], Weichao Jin[a,1], Huisheng Yang[a], Kewei Gao[a], Pengwen Guo[a], Xiaolu Pang[a,*], Alex A. Volinsky[b]

[a] School of Materials Science and Engineering, University of Science and Technology Beijing, Beijing 100083, China
[b] Department of Mechanical Engineering, University of South Florida, Tampa, FL 33620, USA

ARTICLE INFO

Keywords:
Density functional theory
Silicon carbide
Interface
Electronic structure

ABSTRACT

First principles calculations of the SiC/Ti and SiC/Cr interfaces have been conducted based on the density functional theory, and adhesion properties along with the electronic structure were obtained. The crystallographic orientation dependence of the adhesion at the SiC/Ti and SiC/Cr interfaces has been investigated. The work of separation strongly depends on the crystallographic orientation with the SiC(11$\bar{2}$0)/Cr(001) interface having the highest value of W_{sep} = 4.71 J/m^2. By analyzing the electronic structures, it was found that the charge transfer between C and Cr is larger, leading to stronger chemical bonds.

1. Introduction

Ceramic substrates are commonly used as electronic packaging materials with many advantages over plastic and metal counterparts, including good insulation properties, high reliability, thermal and chemical stability [1]. With the rapid development of modern microelectronic technology, the requirements for electronic packaging materials became more stringent, leading to a greater use of ceramic substrates [2]. Silicon carbide (SiC) is a ceramic compound with high thermal conductivity, excellent dielectric properties, high mechanical strength, strong corrosion resistance, thermal and chemical stability and nontoxic nature [3]. For these reasons, SiC is a promising material for electronic packaging [4]. As an electronic packaging material, it is vital for SiC to have a strong interface with metals, which it usually does not [5]. Therefore, studying the interface between SiC and metals is needed. Metal-ceramic interfaces have been studied experimentally via scanning electron microscopy (SEM) and transmission electron microscopy (TEM), which can show microstructure, but not the nature of the atomic scale bonding, along with theoretical aspects [6–7]. Additionally, these interfaces have been studied theoretically via the density functional theory (DFT), which is widely used to explore the nature of bonding and can simultaneously illustrate the electronic structure [8–9].

SiC is a promising material for composites, microelectronics and electronic packaging, and SiC/metal interfaces play an important role in these applications [3]. Considering that the first principles calculations can provide information about the interface at the atomic and electronic scales, one can understand the physical nature of the interface and make reasonable predictions of its performance [10]. This study considers two metals, Ti and Cr, which have been widely used in experiments with SiC [11]. SiC fiber is often used as the reinforcing phase in the Ti matrix composites with strong interfacial bonding properties [12]. Many experiments show that SiC/Cr has strong interfacial bonding because Cr is a strong carbide forming element [13–14]. Ti or Cr used as a transition layer in direct plated copper ceramic substrates can greatly improve the interface adhesion strength compared with no transition layer [15–17]. Therefore, it can be expected that Ti and Cr would have strong interfaces with SiC.

The interfacial adhesion between SiC and other materials, such as graphene, SiO_2, and AlN has been widely studied using the DFT. [18–21] However, little information is available about SiC/metal interfaces, especially the SiC/Cr and SiC/Ti interfaces. Anderson et al. considered the interfacial bonding of α- and β-SiC(0001) with Ti(0001) based on molecular orbital theory, which showed that binding was mainly controlled by the charge transfer from Ti to the half-filled band gap of SiC surface atoms. [22,23] Additionally, the s-p hybridized dangling orbital of the Si and C surfaces forms a chemical bond with 3d Ti, which provides stability of the interfacial system [22,23]. Kohyama and Tanaka et al. studied the SiC/Ti interfaces, interfacial electronic structure and the Schottky barrier heights for new electronic devices applications [24]. Previous experimental studies of the SiC/Cr interface have been conducted, while a few studies have been devoted to

* Corresponding author.
E-mail address: pangxl@mater.ustb.edu.cn (X. Pang).
[1] These authors contributed equally to this work and should be considered first co-authors.

https://doi.org/10.1016/j.microrel.2018.02.019
Received 27 November 2017; Received in revised form 5 February 2018; Accepted 22 February 2018
Available online 20 March 2018
0026-2714/

theoretical research using the DFT. [25–27] The crystallographic orientation dependence of adhesion and electronic structure at the SiC/(Cr, Ti) interface has not been investigated until now.

The first principles investigation of the SiC/(Cr, Ti) interface aids in understanding the nature of the metal-ceramic interfacial adhesion, including factors influencing interfacial bonding, allowing to compare different metals adhered to SiC substrates. However, there is a lack of these in previous literature reports. Thus, we investigated the work of adhesion, atomic and electronic structure of the SiC/(Cr, Ti) interface by using the first principles calculations. In this study, the interface has been formed by many low index crystal surfaces of SiC and Ti or Cr, so that the effect of the crystallographic structure could be examined.

2. Methodology and details

The total energy and electronic structure calculations were performed using the Cambridge serial total energy package (CASTEP), based on the DFT by adopting the plane-wave, ultra-soft pseudopotential method [28,29]. The main purpose of the first principles calculations is to achieve electronic minimization and find the ground state by solving the Kohn-Sham equation with the self-consistent field procedure [30]. The atomic structure minimization is known as geometry optimization by using the Broyden-Fletcher-Goldfarb-Shanno algorithm, where the minimum total energy of the system in achieved. [31] The convergence tolerance was set to $5 \times 10^{-6}\ \frac{eV}{atom}$, with a maximum force of $0.01\ \frac{eV}{Å}$ for geometry optimization. The valence electrons play an important role in this reaction for different atoms. The valence electrons considered in pseudopotentials are Si: $3s^2\ 3p^2$, C: $2s^2\ 2p^2$, Ti: $3s^2\ 3p^6\ 3d^2\ 4s^2$ and Cr: $3s^2\ 3p^6\ 3d^5\ 4s^1$.

The local density approximation (LDA) with the Ceperley-Alder-Perdew-Zunger (CAPZ) functional and the generalized gradient approximation (GGA) with the Perdew-Burke-Ernzerhof (PBE) functional were employed as the exchange-correlation functionals, since both affect calculation accuracy [32]. Since this paper focuses on the interfacial properties, including the SiC/Ti and SiC/Cr interfaces, bulk Ti and SiC, and their surface properties, were first studied by using the first principles calculations. By comparing bulk calculations results with experimental or other computational data, appropriate exchange-correlation functionals and parameters were employed to ensure calculation effectiveness.

The total energy and electronic structure were calculated using the CASTEP code based on the DFT with ultra-soft pseudopotentials, employing the LDA-CAPZ and the GGA-PBE, which were both used to describe interactions in the electronic system [33–35]. The convergence tests were conducted for the plane-wave energy cutoff k-mesh. After sufficient tests, the cutoff energy was set to 350 eV, whether the calculation object is bulk, surface, or an interface. The number of k-points and the sampling of the irreducible wedge of the Brillouin zone gradually increased until good energy convergence, after which it was set to $8 \times 8 \times 8$ for the bulk and $8 \times 8 \times 1$ for the surface and the interface. Silicon carbide also has many structures, and SiC ceramics used as electronic packaging substrates usually have hexagonal close packed structure 4H-SiC.

In order to assess the accuracy of the calculation methods, particularly for the adoption of the appropriate exchange-correlation functionals, a number of calculations of the bulk properties of Ti, Cr and SiC, which provided equilibrium lattice constants ‘a’ or ‘c’, were first performed by the LDA-CAPZ and the GGA-PBE, and the results were compared with others shown in Table 1. Lattice constants calculations are in agreement with previously reported results. Results calculated using the GGA-PBE functional for bulk α-Ti, Cr and 4H-SiC are close to the experimental data, generally corresponding to most other literature reports, which used the GGA-PBE [44–47]. On the contrary, the values calculated with the LDA-CAPZ are consistently overestimated by at least 10%. Therefore, the GGA-PBE exchange-correlation functional was selected to perform the calculations in this paper.

Table 1
Theoretically predicted and measured lattice constants of Ti, Cr and SiC.

System	Lattice constant		Reference
	a, Å	$\frac{c}{a}$	
Ti	2.869	1.578	This study, LDA
	2.946	1.576	This study, GGA
	2.752	1.585	Ref. [36], LDA
	2.94	1.587	Ref. [37], GGA
	2.95	1.587	Ref. [38], experiment
Cr	2.794		This study, LDA
	2.851		This study, GGA
	2.779		Ref. [39], LDA
	2.836		Ref. [39], GGA
	2.884		Ref. [40], experiment
SiC	3.04	3.274	This study, LDA
	3.084	3.277	This study, GGA
	3.039	3.283	Ref. [41], LDA
	3.089	3.273	Ref. [42], GGA
	3.078	3.277	Ref. [43], experiment

The material surface was modeled as a slab, which should be thick enough to ensure bulk-like behavior, primarily because more atomic layers will yield more accurate results. At the same time, more atomic layers take longer computing time. Accordingly, we first determined the minimum number of atomic layers depending on the chemical or physical properties of the surface slab. For transition metals, a slab thickness of 10 Å is usually sufficient to ensure bulk-like properties inside the slab [48]. Cr surface and Ti surface models were built using the 6-layers slab. SiC surface of primary crystallographic orientation contains more than eight atomic layers [49]. The interface combined with the supercell model contained two free surfaces of the metal and the SiC slab per period separated by a 10 Å vacuum layer.

Generally, the surface free energy (σ_{surf}) for the slab can be obtained from [50]:

$$\sigma_{surf} = [E_{slab}(N) - N\Delta E] \quad (1)$$

Here, $E_{slab}(N)$ is the total energy of the surface slab, N is the total number of surface atoms in the slab, ΔE is the average energy of ${E_{slab}}^{N}$ and ${E_{slab}}^{N-2}$. Since the SiC surface is either Si-terminated or C-terminated, the surface energy could not be obtained from Eq. (1) if both sides of the surface are the same single element, due to odd-numbered slab and deviation from stoichiometry. The surface energy of an odd-numbered slab should consider the corresponding chemical element in Eq. (1). The surface energy can be quickly calculated for an even-numbered slab ensuring that the slab preserves its stoichiometry. However, the SiC slab has C- and Si-terminated surfaces at the top and the bottom simultaneously, thus the calculated surface energy is an average of the two terminations according to Eq. (1).

In this work, the surface energy with primary orientation was calculated, listed in Table 2. Due to lower Miller indices, highly stable crystallographic orientations can be selected. The surface energy of Cr,

Table 2
Calculated surface energy of main crystallographic planes for Ti, Cr and SiC.

System	Structure	Orientation	Surface energy, J/m^2
α-Ti	hcp	(0001)	1.7243
		$(10\bar{1}0)$	1.9401
		$(11\bar{2}0)$	1.7493
Cr	bcc	(001)	3.4381
		(110)	2.8695
		(111)	3.3981
4h-SiC	hcp	(0001)	5.9849
		$(10\bar{1}0)$	3.4502
		$(11\bar{2}0)$	2.6911

Ti and SiC slabs is $\sigma_{surf}^{Ti}(0001) = 1.7243\ J/m^2$,$\sigma_{surf}^{Cr}(110) = 2.8695\ J/m^2$ and $\sigma_{surf}^{SiC}(11\bar{2}0) = 2.6911\ J/m^2$, respectively, indicating relative stability. Based on previous research, the lowest surface energy for metal is often obtained by the close-packed plane, in agreement with calculated results in Table 2 [51]. However, the surface energy of SiC depends on the surface dangling bonds. Previous research indicated that stable surface will affect interfacial adhesion. Hence, this article also attempts to carry out an exploration of the relation between the surface energy and interfacial adhesion [52].

3. Results and discussion

3.1. The work of separation

The work of separation, W_{sep}, can be used to quantitatively describe adhesion strength of the metal-ceramic interface, which is defined as the reversible work to separate a unit area interface of the two condensed phases, forming two free surfaces, given by [53]:

$$W_{sep} = \frac{E_{slab,\ \alpha} + E_{slab,\beta} - E_{int}}{A} \quad (2)$$

Here, $E_{slab,\ \alpha}$ and $E_{slab,\ \beta}$ is the total energy of the surface slab and the subscripts α and β are materials α and β. E_{int} is the total energy of the interface and A is the interface area.

The interface structure of six SiC/Ti interfaces is shown in Fig. 1. Separation distance, d_0, greatly affects W_{sep} and inter-atomic bonding, thus we've selected 1.5–2 Å for d_0 [54,55]. Furthermore, the lattice plane of the 4H-SiC has two different atomic terminations: Si and C. Interfacing the C-terminated surface with a metal, such as Ti and Cr, has been proven to be much stronger. Therefore, this paper provides the DFT study of the interfacial properties.

Table 3
Work of separation W_{sep} for Ti/SiC with the main crystallographic plane.

Ceramic surface	Metal surface	W_{sep}
SiC	Ti	J/m^2
(0001)	(0001)	0.3263
	$(10\bar{1}0)$	0.3057
	$(11\bar{2}0)$	–
$(10\bar{1}0)$	(0001)	0.3132
	$(10\bar{1}0)$	0.1784
	$(11\bar{2}0)$	–
$(11\bar{2}0)$	(0001)	0.3118
	$(10\bar{1}0)$	–
	$(11\bar{2}0)$	0.1452

Table 3 shows the W_{sep} for SiC/Ti with (0001)/$(11\bar{2}0)$, $(10\bar{1}0)$/$(11\bar{2}0)$ and $(11\bar{2}0)$/$(10\bar{1}0)$ interfaces not forming at all. This is due to the big difference between the structures for those surfaces, resulting in a large mismatch. To understand the relationship between the adhesion strength and the surface energy of the Ti(0001)/SiC interfaces, we selected (0001)/(0001), (0001)/$(10\bar{1}0)$ and (0001)/$(10\bar{2}0)$ orientations combinations, shown in Fig. 1 along with a linear fit. This graph provides a relationship between the surface energy σ and W_{sep} for different SiC planes forming interfaces with the same Ti(0001) surface. Based on Fig. 2, there's a linear relationship between W_{sep} and increasing surface energy.

The interface structure of four SiC/Cr interfaces is shown in Fig. 3. Due to the large mismatch induced by different structures, only four of

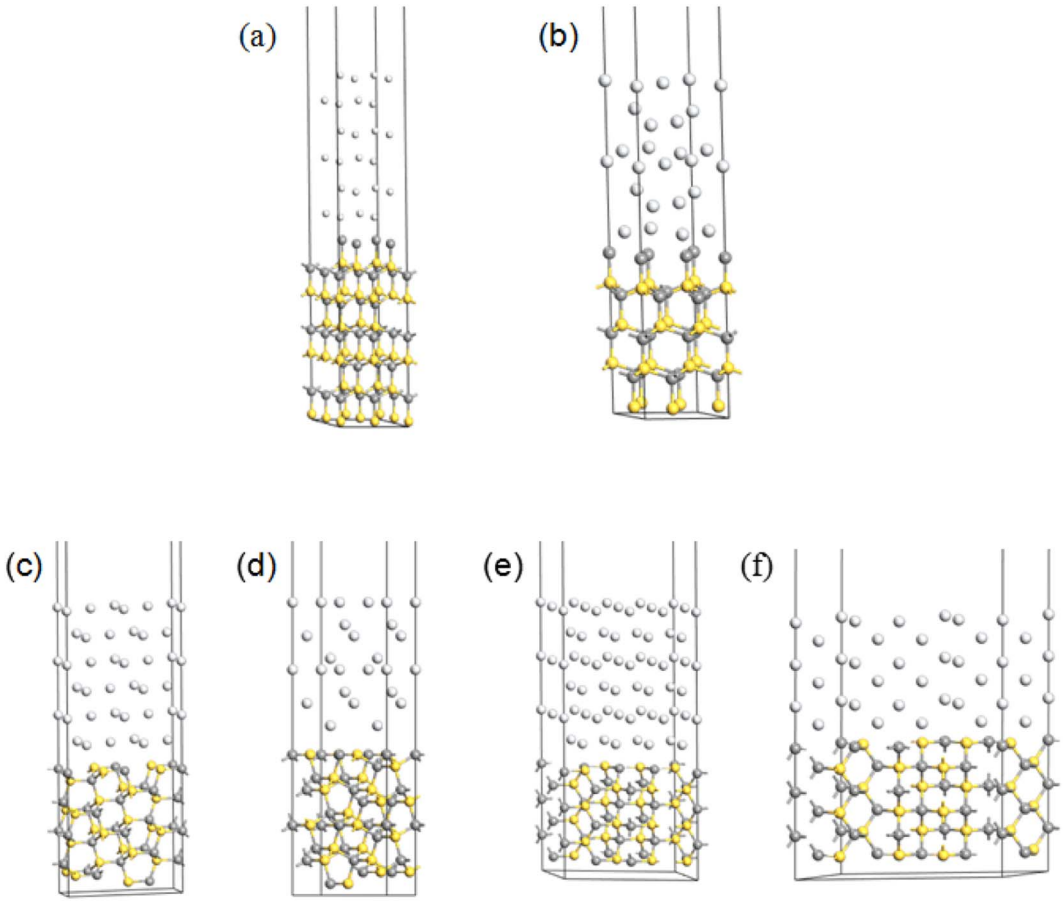

Fig. 1. Interface structures of (a) SiC(0001)/Ti(0001), (b) SiC(0001)/Ti($10\bar{1}0$), (c) SiC($10\bar{1}0$)/Ti(0001), (d)SiC($10\bar{1}0$)/Ti($10\bar{1}0$), (e) SiC($11\bar{2}0$)/Ti(0001), (f) SiC($11\bar{2}0$)/Ti ($11\bar{2}0$). (Silver: titanium; grey: carbon; yellow: silicon). (For interpretation of the references to colour in this figure legend, the reader is referred to the web version of this article.)

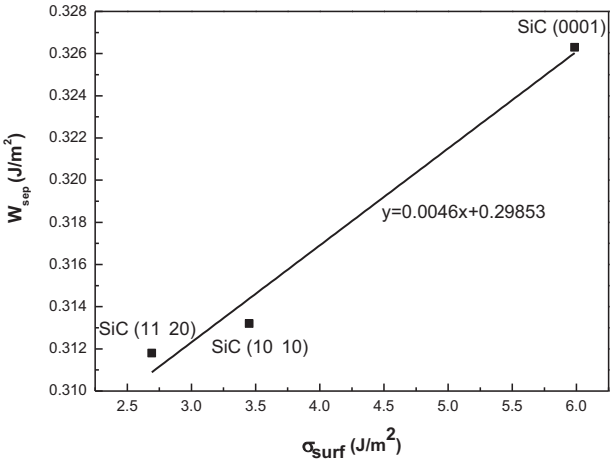

Fig. 2. Relationship between the surface energy σ and W_{sep} for SiC/Ti(0001) interface. The black data points represent calculated results, and the line is the linear fit.

nine interfaces had adhesion, as shown in Table 4. The maximum W_{sep} is 4.7108 J/m^2 for the $SiC(11\bar{2}0)/Cr(001)$ interface. The interface in this orientation has good stability, and has potential to be used for helping experiments. Based on these results, adhesion at the SiC/Ti and SiC/Cr interfaces strongly depends on the crystallographic orientation.

3.2. Interfacial structure and interfacial energy

3.2.1. Interface structure

To understand how the interface reaches its stable structure and reduce the interfacial energy, it is necessary to find how atoms move. The unrelaxed and relaxed local structures for $SiC(0001)/Ti(0001)$ and $SiC(11\bar{2}0)/Cr(001)$ interfaces are given in Fig. 4.

Form Fig. 4, it is obvious that there are substantial changes in the atomic geometry of the relaxed interface. After relaxation, it can be found that the atomic restructure degree at Ti layer is slight, as only the first layer close to the interface has changed, but Cr layer has changed significantly. In Fig. 4, after structure relaxation, the SiC(0001)/Ti (0001) interface spacing has changed a lot from 2.076 Å to 0.955 Å, and the SiC(11$\bar{2}$0)/Cr(001) interface spacing also changed from 1.864 Å to 1.692 Å. Moreover, in unrelaxed SiC(0001)/Ti(0001), the C—Si bond length and C—Si—C bond angle at the interface are 1.904 Å and 110.13°,while after structural relaxation, they changed to 1.874 Å and 110.84°, which are extremely small changes. Form Fig. 4(c) and (d), it is clear that compared with the unrelaxed interface, relaxed $SiC(11\bar{2}0)/Cr(001)$ has undergone strong atomic rearrangements at the interface. The C—Si bond length and C—Si—C bond angle at the interface transformed to 1.874 Å and 110.84° from 1.904 Å and 110.13°. The

Table 4
Work of separation W_{sep} for Cr/SiC with the main crystallographic plane.

Ceramic surface	Metal surface	W_{sep}
SiC	Cr	J/m^2
(0001)	(111)	2.528
(10$\bar{1}$0)	(001)	2.859
(11$\bar{2}$0)	(001)	4.711
(11$\bar{2}$0)	(110)	2.326

SiC(11$\bar{2}$0)/Cr(001) with strongly reconstruction could greatly reduce the system energy, thus it is necessary to make sure that the interface structure is in steady state.

3.2.2. Interface energy

Another thermodynamic quantity, which can be used to represent interfacial thermodynamic stability, is the interfacial energy, γ_{int}. It can be defined as the excess free energy associated with the unit area of the system due to the interface forming, and comes from the charge transfer between the interface atoms and the structure strain. It is difficult to obtain precise interfacial energy from experiments; therefore only approximate value can be assessed. In many cases of solid/solid interfaces, γ_{int} has been ignored, or set to zero when both solid structures are similar. Due to the interfacial misfit strain caused by different structures, interfacial energy should be positive. However, it can also be negative under some conditions, which are not thermodynamically stable. The atoms at the interface region will diffuse across the interface, and begin interfacial alloying when the interfacial energy is negative enough. The smaller the interface, the steadier it is. The interfacial energy is defined as [56]:

$$\gamma_{int} = \frac{E_{\alpha/\beta}(N,M) - NE_{\alpha}^{bulk} - ME_{\beta}^{bulk}}{A_i} - \gamma_{\alpha} - \gamma_{\beta} \quad (3)$$

Here, γ_{α} and γ_{β} are the surface energy of materials α and β, respectively; $E_{\alpha/\beta}$, NE_{α}^{bulk} and NE_{β}^{bulk} are the total energy of the interface system, the energy of bulk α and bulk β per atom, respectfully; A_i is the area of the interface, and N and M are the atomic numbers of materials α and β, respectively. $SiC(0001)/Ti(0001)$ and $SiC(11\bar{2}0)/Cr(001)$ have the highest stability for the SiC/Ti and SiC/Cr interfaces, with their interfacial energy listed in Table 5. Table 5 also shows that for the latter, W_{sep} is smaller, while γ_{int} is larger than for the former. This means that the smaller γ_{int} will result in larger W_{sep}, and both contribute to the interface stability in different ways.

3.3. Electronic structure

In the previous section it was found that the optimal orientations for

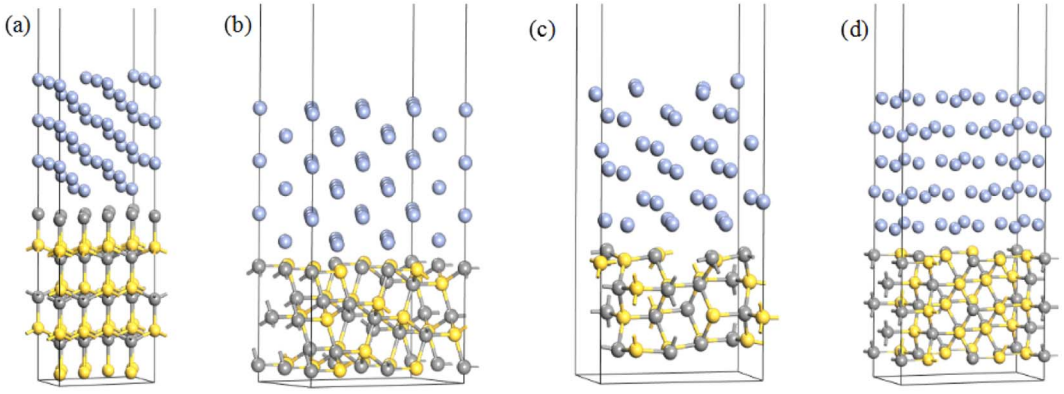

Fig. 3. Interface structures of: (a) SiC(0001)/Cr(111), (b) SiC(10$\bar{1}$0)/Cr(001), (c) SiC(11$\bar{2}$0)/Cr(001), (d) SiC(11$\bar{2}$0)/Cr(110). (Green: chromium; silver: titanium; grey: carbon; yellow: silicon). (For interpretation of the references to colour in this figure legend, the reader is referred to the web version of this article.)

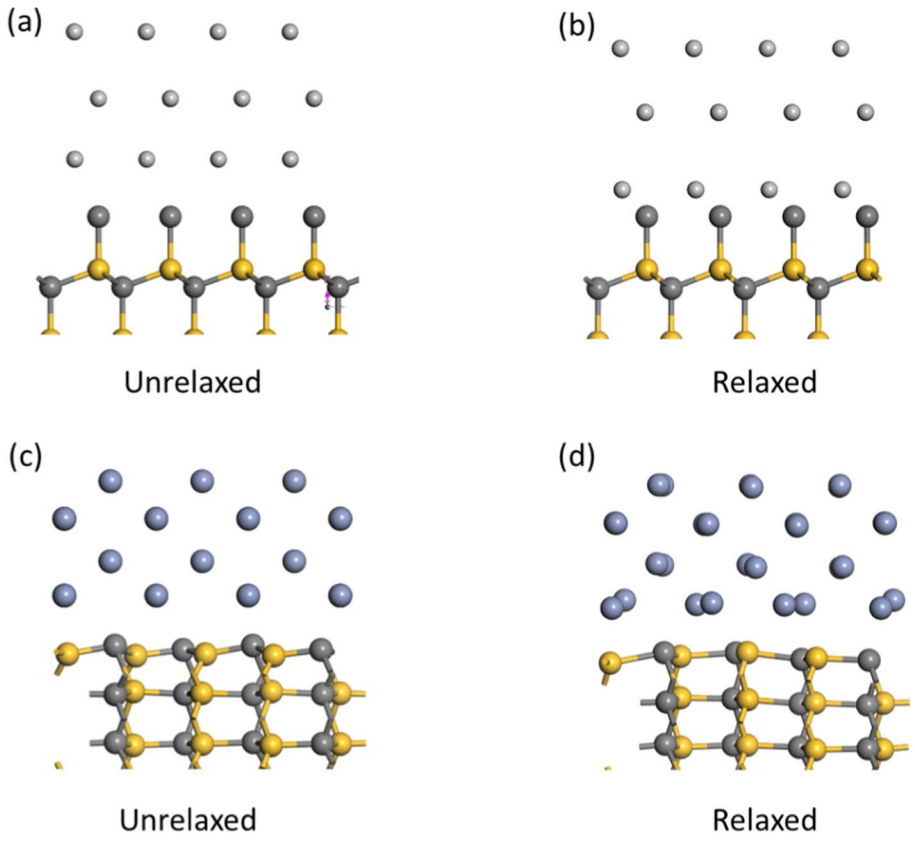

Fig. 4. Unrelaxed and relaxed local atomic structures for: (a) unrelaxed *SiC*(0001)/*Ti*(0001) interface, (b) relaxed *SiC*(0001)/*Ti*(0001) interface, (c) unrelaxed *SiC*$(11\bar{2}0)$/*Cr*(001) interface, (d) relaxed *SiC*$(11\bar{2}0)$/*Cr*(001) interface.

Table 5
Best interfacial energies W_{sep} and γ_{int} for the SiC/Ti and SiC/Cr models.

Interface model	Best orientation	W_{sep}	γ_{int}
		J/m^2	J/m^2
SiC/Ti	(0001)/(0001)	0.3263	2.4806
SiC/Cr	$(11\bar{2}0)$/(001)	4.7108	1.4344

the SiC/Cr and SiC/Ti interfaces are *SiC*$(11\bar{2}0)$/*Cr*(001) and *SiC*(0001)/*Ti*(0001), respectively. To better understand these two interfaces, it is necessary to perform the deformation density, the Mulliken population and the density of states (DOS) calculations, which all depend on electronic interactions.

Fig. 5 shows the interface geometry of *SiC*$(11\bar{2}0)$/*Cr*(001) and *SiC*(0001)/*Ti*(0001). The former only has C-terminated SiC surface, while both C-terminated SiC and Si-terminated SiC surfaces are present for the latter. The C—Cr and Si—Cr bonds formed at the *SiC*$(11\bar{2}0)$/*Cr*(001) interface enhance the charge interactions between C and Si, possibly due to the Si atom, which will be discussed later.

For better understanding of electronic interactions and chemical bonds, the valence electron density difference for the *SiC*$(11\bar{2}0)$/*Cr*(001) and *SiC*(0001)/*Ti*(0001) interfaces is shown in Fig. 6. Red and blue areas represent charge increase and decrease, respectively. The charge accumulates primarily in the areas around C atoms, implying that electron transfer occurs at the interface. There are two visible differences between the two interfaces. First, the charge transfer at the SiC$(11\bar{2}0)$/Cr(001) interface is shown in Fig. 6(b), where the charge transfers mainly from Cr to C atoms, stronger than the charge transfer at the SiC(0001)/Ti(0001) interface. Thus, stronger chemical bonds have formed between the C and Cr atoms, in agreement with the W_{sep} variations in Table 4. A distinct charge transfer occurs at both interfaces, suggesting that the ionic bond has formed. Second, for the Si atom shown in Fig. 6(b), one part of the charge has been transferred to the C atom, while the other part has been shared with the Cr atom at the *SiC*(0001)/*Ti*(0001) interface. Therefore, the electrostatic force between the Cr and C atoms has been enhanced by the Si atom. Moreover, a covalent bond can be found between the neighboring Si and Cr atoms. Since they share some electrons, this also strengthens the interface bonding for the SiC$(11\bar{2}0)$/Cr(001) interface.

A figure of the valence electron density difference can show the charge transfer and the degree of ionization of the interface system, but not quantitatively. Therefore, the Mulliken charge population has been used, which may help to understand this quantitatively. Table 6 shows the charges for the *SiC*$(11\bar{2}0)$/*Cr*(001) and *SiC*(0001)/*Ti*(0001) interfaces. Almost all the change in the Mulliken population appeared at the ceramic layer and the interface. In order to analyze the charge transfer at the interface, we selected interfacial atoms, including C, Si, Cr and Ti in order to look more closely at the Mulliken population. Table 6 indicates that the charge transfer from the metal layer to the ceramic layer is clear, about 1.07 electrons for the *SiC*$(11\bar{2}0)$/*Cr*(001) interface, and 0.9 electrons for the *SiC*(0001)/*Ti*(0001) interface, showing the existence of ionic interaction at the interface. In addition, some Si and Cr atoms had no charge transfer, implying that covalent bonds may exist, which is in agreement with the electron density difference.

Fig. 7 shows the total DOS and partial DOS of the selected atoms for the two interfaces. The interfacial Ti atoms have the same electronic state as bulk Ti atom, while the peak of the DOS for the interfacial Ti becomes sharper, as shown in Fig. 7(a). This implies that electrons became localized. The DOS of the interfacial Cr, C and Si atoms are very similar to their corresponding atoms in the bulk. In addition, the interfacial Ti atom shows a set of new states at around −10 eV, which is a result of the surface effect and is called the surface level. In Fig. 7(a), orbital hybridizations can be analyzed. C and Ti atoms of the interface

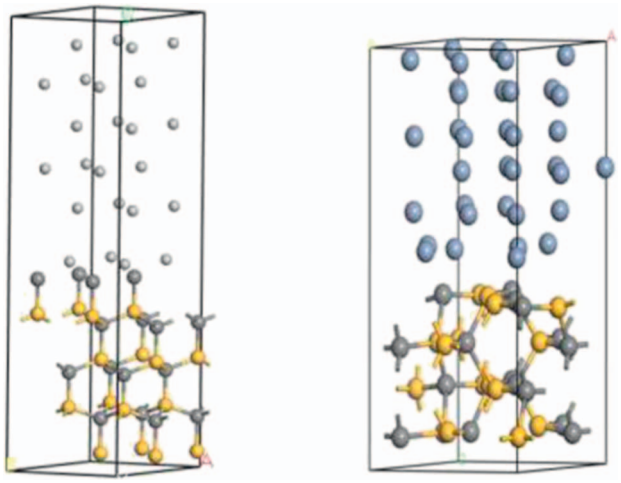

(a) SiC(0001)/Ti(0001) interface (b)SiC(11$\bar{2}$0)/Cr(001) interface

Fig. 5. Relaxed interface geometry for: (a) *SiC*(0001)/*Ti*(0001) and (b) *SiC*(11$\bar{2}$0)/*Cr*(001). (Green: chromium; silver: titanium; grey: carbon; yellow: silicon). (For interpretation of the references to colour in this figure legend, the reader is referred to the web version of this article.)

have the same peak in DOS with the energy ranging from −5 to 0 eV, which indicates the presence of the C-2p/Ti-3d orbital hybridization and a covalent bond can be seed for Fig. 7(c). Similarly, in Fig. 7(d), the Cr-3d/C-2p and Cr-3d/Si-2p at interfacial area have hybridization interactions, which means that Cr—C and Cr—Si also have covalent bonding due to the overlap of the peaks between Cr and C. Cr and Si also present in the −5 to 0 eV energy range, as shown in the Fig. 7(b). Comparing Fig. 7(a) and (b), the overlapping area in Fig. 4(a) for interfacial Ti and C has less than one of the interfacial Cr and C atoms from Fig. 7(b), which means that the strength of the Ti—C bond is weaker than the Cr—C bond.

4. Conclusions

The first principles calculations, based on the DFT were performed to explore the adhesion properties of the SiC/Ti and SiC/Cr interfaces in various orientations. Considering mismatches between the two constituent surfaces, six interface models of SiC/Ti and four interface models of SiC/Cr have been successfully built. The optimized geometry, work of separation, interfacial energy, electron density difference, the Mulliken population and the density of states for the interface models were calculated. The following conclusions can be drawn:

Table 6
The Mulliken charges for the *SiC*(11$\bar{2}$0)/*Cr*(001) and *SiC*(0001)/*Ti*(0001) interfaces.

Interface	Element	s	p	d	Total	Charge, e
SiC/Cr	C	1.45	3.62	0	5.07	−1.07
	Si	1.13	2.04	0	3.17	0.83
	Cr	2.38	6.64	5.02	13.86	0.14
SiC/Ti	C	1.5	3.41	0	4.9	−0.9
	Ti	2.25	6.48	2.57	11.31	0.69

(1) Calculation of the work of separation for interfaces formed by various planes of SiC, Ti and Cr indicate that the optimal orientation for the SiC/Ti interface is *Ti*(0001)/*SiC*(0001), which has the highest value of W_{sep} = 0.3263 J/m^2. Similarly, the optimal orientation for the SiC/Cr interface is *SiC*(11$\bar{2}$0)/*Cr*(001) with W_{sep} = 4.7108 J/m^2. The W_{sep} for *SiC*(11$\bar{2}$0)/*Cr*(001) is larger than for *Ti*(0001)/*SiC*(0001), which suggests that the *SiC*(11$\bar{2}$0)/*Cr*(001) interface has the strongest adhesion and is the most stable.
(2) The interfacial energy calculations for *SiC*(11$\bar{2}$0)/*Cr*(001) and *SiC*(0001)/*Ti*(0001) show that the smaller γ_{int} will result in larger W_{sep}. In addition, the DFT calculations of W_{sep} and interfacial energy suggest that the crystallographic orientation should

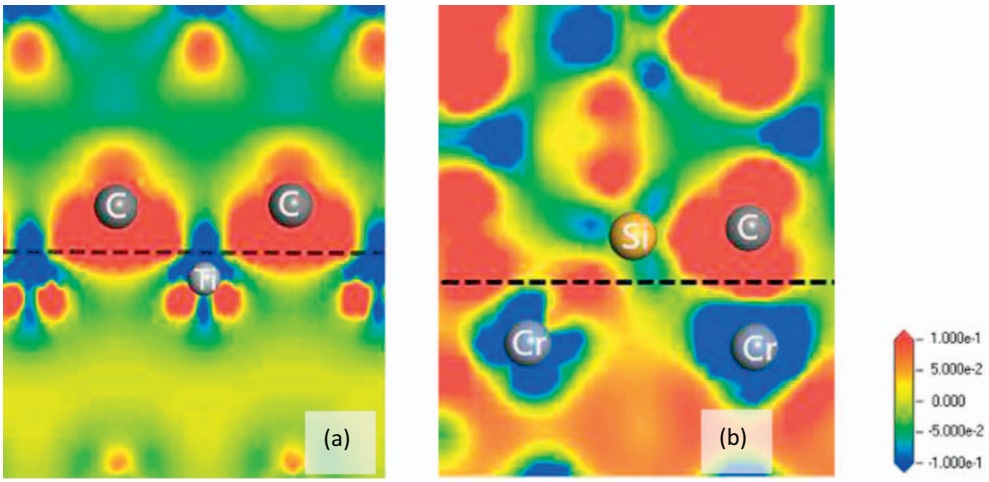

Fig. 6. Valence electron density difference along the plane containing different interfacial C, Si and Ti or Cr atoms at the interface for: (a) *SiC*(0001)/*Ti*(0001) and (b) *SiC*(11$\bar{2}$0)/*Cr*(001). Dotted line indicates the interface location.

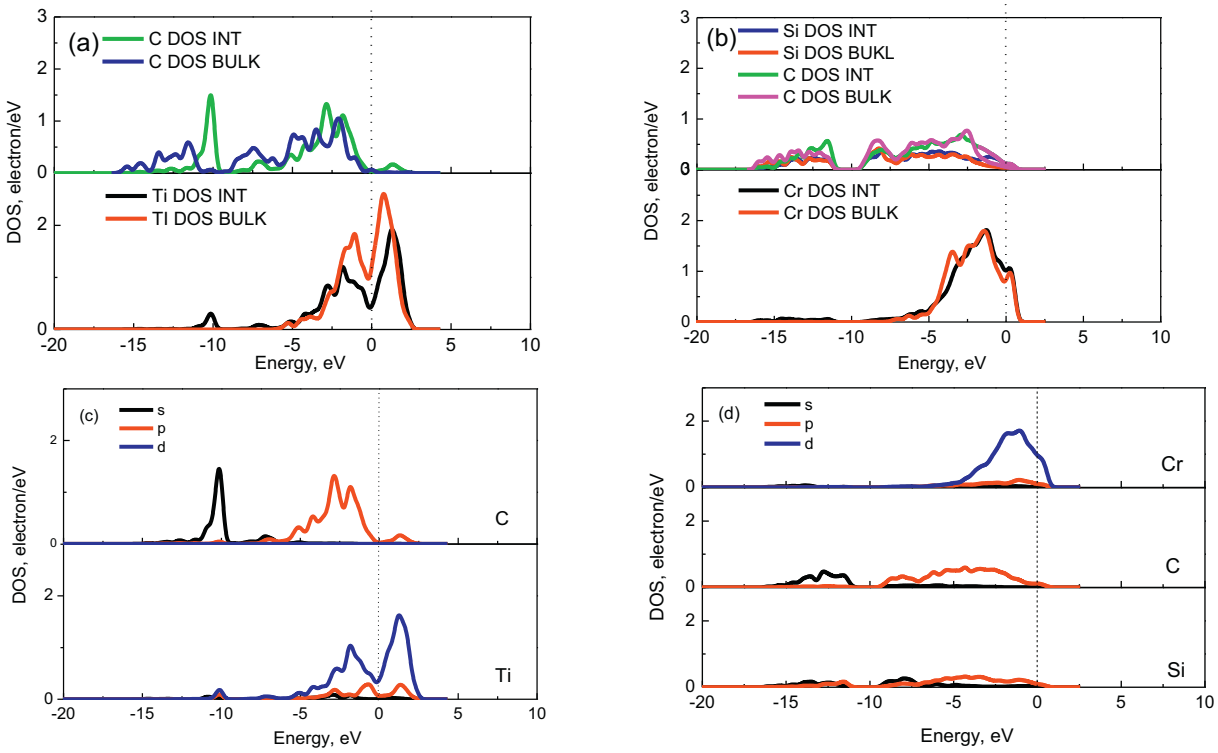

Fig. 7. Total DOS for selected atoms at interfaces: (a) *SiC*(0001)/*Ti*(0001) and (b) *SiC*(11$\bar{2}$0)/*Cr*(001). Partial DOS for selected atoms at interface region: (a) partial DOS of C and Ti atom at the *SiC*(0001)/*Ti*(0001) interface, (b) partial DOS of Cr, C and Si atom at the *SiC*(11$\bar{2}$0)/*Cr*(001). "INT" means the atom at the interface. "BULK" means the atom in the bulk. Vertical dotted lines show the location of the Fermi energy.

significantly affect the interface bonding.

(3) The relationship between the surface energy and W_{sep} was obtained, showing a positive relationship between the SiC surface energy and the value of W_{sep} for interfaces formed by SiC surfaces with different orientations and the Ti(0001) surface.

(4) According to the study of the electronic structure, it was found that a covalent bond can be formed between the neighboring Si and Cr atoms for *SiC*(11$\bar{2}$0)/*Cr*(001), which strengthens the interface bonding. Moreover, the charge transfer of *SiC*(11$\bar{2}$0)/*Cr*(001) is mainly from Cr to C atoms and is stronger than from Ti to C at the *SiC*(0001)/*Ti*(0001) interface. Thus, the stronger chemical bond has formed between C and Cr atoms, which agrees with W_{sep} variations in Tables 3 and 4. From the Mulliken population, one can see that the ionic interaction at the interface exists and ionic bonding between Cr and C is stronger than between Ti and C. From the DOS, the overlapping area in Fig. 4(a) for interfacial Ti and C has less than one interfacial Cr and C in Fig. 4(b), which means that the strength of the Ti—C bond is weaker than the Cr—C bond.

Acknowledgements

This work was supported by the Beijing Nova Program (Z171100001117075), the National Natural Science Foundation of China (51771025), and the Fundamental Research Funds for the Central Universities (FRF-TP-17-002C1).

References

[1] S. Pietranico, S. Pommier, S. Lefebvre, Z. Khatir, S. Bontemps, Characterisation of power modules ceramic substrates for reliability aspects, Microelectron. Reliab. 49 (9–11) (2009) 1260–1266.
[2] N. Chasserio, S. Guillemet-Fritsch, T. Lebey, S. Dagdag, Ceramic substrates for high-temperature electronic integration, J. Electron. Mater. 38 (1) (2009) 164–174.
[3] S. Zhu, S. Ding, R. Wang, Low-temperature fabrication of porous SiC ceramics by preceramic polymer reaction bonding, Mater. Lett. 59 (5) (2005) 595–597.
[4] G.L. Harris (Ed.), Properties of Silicon Carbide (EMIS Data Reviews Series vol 13), INSPEC, London, 1995, pp. 235–237.
[5] A.J. Fischer, A.A. Allerman, M.H. Crawford, K.H.A. Bogart, S.R. Lee, R.J. Kaplar, Room-temperature direct current operation of 290 nm light-emitting diodes with milliwatt power levels, Appl. Phys. Lett. 84 (17) (2004) 3394–3396.
[6] I.E. Reimanis, B.J. Dalgleish, A.G. Evans, The fracture resistance of a model metal/ceramic interface, Acta Metall. Mater. 39 (12) (1991) 3133–3141.
[7] M. Christensen, S. Dudiy, G. Wahnström, First-principles simulations of metal-ceramic interface adhesion: Co/WC vs Co/TiC//APS meeting, APS Meeting Abstracts, 2001.
[8] M. Levy, Universal variational functionals of electron densities, first-order density matrices, and natural spin-orbitals and solution of the v-representability problem, Proc. Natl. Acad. Sci. 76 (12) (1979) 6062–6065.
[9] M.W. Finnis, The theory of metal-ceramic interfaces, J. Phys. Condens. Matter 8 (32) (1996) 5811.
[10] R. Leucht, H.J. Dudek, Properties of SiC-fibre reinforced titanium alloys processed by fibre coating and hot isostatic pressing, Mater. Sci. Eng. A 188 (1–2) (1994) 201–210.
[11] Y.Q. Yang, Y. Zhu, Z.J. Ma, Y. Chen, Formation of interfacial reaction products in SCS-6 SiC/Ti2AlNb composites, Scr. Mater. 51 (5) (2004) 385–389.
[12] X.H. Lü, Y.Q. Yang, C.X. LIU, C.H.E.N. Yan, Y.L. AI, Kinetics and mechanism of interfacial reaction in SCS-6 SiC continuous fiber-reinforced Ti-Al intermetallic matrix composites, Trans. Nonferrous Metals Soc. China 16 (1) (2006) 77–83.
[13] M. Niibe, M. Mukai, H. Kimura, Y. Shoji, Polarization property measurement of the long undulator radiation using Cr/C multilayer polarization elements, Am. Inst. Phys. Conf. Proc. (2004) 243–246.
[14] G.X. Jia, Y. Li, H.T. Li, P.F. Hu, X. Zhang, B.L. Jiang, Study on mechanical properties and preparation of self-lubricating Cr/C composite coatings, J. Funct. Mater. 41 (7) (2010) (1150-1153+1157).
[15] T. Yamasaki, N. Tajima, T. Kaneko, N. Nishikawa, J. Nara, T. Schimizu, ... T. Ohno, 4H-SiC Surface Structures and Oxidation Mechanism Revealed by Using First-Principles and Classical Molecular Dynamics Simulations. Materials Science Forum, 858 Trans Tech Publications, 2016, pp. 429–432.
[16] B. Lu, F.R. Hyatt, R.P. Petit, B.C. Tseng, Direct plated copper (DPC) used in wireless product (high frequency) applications, SPIE Proceedings Series, Society of Photo-Optical Instrumentation Engineers, 2000, pp. 479–484.
[17] A. Kondo, T. Oogami, K. Sato, Y. Tanaka, Structure and properties of cathodic arc ion plated CrN coatings for copper machining cutting tools, Surf. Coat. Technol. 177 (2004) 238–244.
[18] F. Varchon, R. Feng, J. Hass, X. Li, B.N. Nguyen, C. Naud, Electronic structure of epitaxial graphene layers on SiC: effect of the substrate, Phys. Rev. Lett. 99 (12) (2007) 126805.
[19] J.M. Knaup, P. Deák, T. Frauenheim, A. Gali, Z. Hajnal, W.J. Choyke, Defects in SiO_2 as the possible origin of near interface traps in the SiC/SiO_2 system: a systematic theoretical study, Phys. Rev. B 72 (11) (2005) 115323.
[20] P. Deák, A. Gali, J. Knaup, Z. Hajnal, T. Frauenheim, P. Ordejón, J.W. Choyke,

Defects of the SiC/SiO_2 interface: energetics of the elementary steps of the oxidation reaction, Phys. B Condens. Matter 340 (2003) 1069–1073.
[21] A. Rizzi, R. Lantier, F. Monti, H. Lüth, F.D. Sala, A. Di Carlo, P. Lugli, AlN and GaN epitaxial heterojunctions on 6H–SiC (0001): valence band offsets and polarization fields, J. Vac. Sci. Technol., B: Microelectron. Nanometer Struct.–Process., Meas., Phenom. 17 (4) (1999) 1674–1681.
[22] A.B. Anderson, C. Ravimohan, Bonding of α-SiC basal planes to close-packed Ti, Cu, and Pt surfaces: molecular-orbital theory, Phys. Rev. B 38 (2) (1988) 974.
[23] S.P. Mehandru, A.B. Anderson, Adhesion and bonding of polar and non-polar SiC surfaces to Ti (0001), Surf. Sci. 245 (3) (1991) 333–344.
[24] S. Tanaka, M. Kohyama, Ab initio calculations of the 3C-SiC (111)/Ti polar interfaces, Phys. Rev. B 64 (23) (2001) 235308.
[25] M. Huang, K.Z. Li, H.J. Li, Q.G. Fu, G.D. Sun, Double-layer oxidation protective SiC/Cr–Al–Si coating for carbon–carbon composites, Surf. Coat. Technol. 201 (18) (2007) 7842–7846.
[26] M. Naka, J.C. Feng, J.C. Schuster, Phase reactions and diffusion path of the SiC/Cr system, J. Mater. Synth. Process. 6 (3) (1998) 169–173.
[27] K.L. Moazed, Metal/semiconductor interfacial reactions, Metall. Trans. A. 23 (7) (1992) 1999–2006.
[28] M.D. Segall, P.J. Lindan, M.A. Probert, C.J. Pickard, P.J. Hasnip, S.J. Clark, M.C. Payne, First-principles simulation: ideas, illustrations and the CASTEP code, J. Phys. Condens. Matter 14 (11) (2002) 2717.
[29] D. Vanderbilt, Soft self-consistent pseudopotentials in a generalized eigenvalue formalism, Phys. Rev. B 41 (11) (1990) 7892.
[30] W. Kohn, Density functional and density matrix method scaling linearly with the number of atoms, Phys. Rev. Lett. 76 (17) (1996) 3168.
[31] T.H. Fischer, J. Almlof, General methods for geometry and wave function optimization, J. Phys. Chem. 96 (24) (1992) 9768–9774.
[32] J.P. Perdew, E.R. Mcmullen, A. Zunger, Density-functional theory of the correlation energy in atoms and ions: a simple analytic model and a challenge, Phys. Rev. A 23 (6) (1981) 2785–2789.
[33] J.P. Perdew, A. Zunger, Self-interaction correction to density-functional approximations for many-electron systems, Phys. Rev. B 23 (10) (1981) 5048.
[34] D.M. Ceperley, B.J. Alder, Ground state of the electron gas by a stochastic method, Phys. Rev. Lett. 45 (7) (1980) 566.
[35] J.P. Perdew, K. Burke, M. Ernzerhof, Generalized gradient approximation made simple, Phys. Rev. Lett. 77 (18) (1996) 3865.
[36] M.N. Huda, L. Kleinman, Density functional calculations of the influence of hydrogen adsorption on the surface relaxation of Ti (0001), Phys. Rev. B 71 (24) (2005) 241406.
[37] N.L. Allinger, M.J. Hickey, Acetone, ab initio calculations, Tetrahedron 28 (8) (1972) 2157–2161.
[38] C. Kittel, C. Fong, Quantum Theory of Solids, Wiley, New York, 1963.
[39] R. Hafner, D. Spišák, R. Lorenz, J. Hafner, Magnetic ground state of Cr in density-functional theory, Phys. Rev. B 65 (18) (2002) 184432.
[40] V.L. Moruzzi, P.M. Marcus, Antiferromagnetism in 3d transition metals, Phys. Rev. B 42 (13) (1990) 8361.
[41] M. Posselt, F. Gao, W.J. Weber, Atomistic simulations on the thermal stability of the antisite pair in 3C-and 4H-SiC, Phys. Rev. B 73 (12) (2006) 125206.
[42] T. Yamasaki, N. Tajima, T. Kaneko, N. Nishikawa, J. Nara, T. Schimizu, ... T. Ohno, 4H-SiC Surface Structures and Oxidation Mechanism Revealed by Using First-Principles and Classical Molecular Dynamics Simulations. Materials Science Forum, 858 Trans Tech Publications, 2016, pp. 429–432.
[43] P. Käckell, B. Wenzien, F. Bechstedt, Influence of atomic relaxations on the structural properties of SiC polytypes from ab initio calculations, Phys. Rev. B 50 (23) (1994) 17037.
[44] I. Dontas, S. Karakalos, S. Ladas, S. Kennou, Study of the early stages of Cr/4H-SiC(11-20) interface formation and its behavior at high temperatures, Phys. Status Solidi 5 (12) (2008) 3744–3747.
[45] K. Nobuhara, H. Nakayama, M. Nose, S. Nakanishi, H. Iba, First-principles study of alkali metal-graphite intercalation compounds, J. Power Sources 243 (2013) 585–587.
[46] W. Liu, J.C. Li, W.T. Zheng, Q. Jiang, Ni Al (110)/Cr (110) interface: a density functional theory study, Phys. Rev. B 73 (20) (2006) 205421.
[47] S. Lutfalla, V. Shapovalov, A.T. Bell, Calibration of the DFT/GGA + U method for determination of reduction energies for transition and rare earth metal oxides of Ti, V, Mo, and Ce, J. Chem. Theory Comput. 7 (7) (2011) 2218–2223.
[48] W.T. Geng, Cr segregation at the Fe-Cr surface: a first-principles GGA investigation, Phys. Rev. B 68 (23) (2003) 233402.
[49] H. Li, Y.I. Matsushita, M. Boero, A. Oshiyama, First-principles calculations that clarify energetics and reactions of oxygen adsorption and carbon desorption on 4H-SiC ($11\bar{2}0$) surface, J. Phys. Chem. C 121 (7) (2017) 3920–3928.
[50] V. Fiorentini, M. Methfessel, Extracting convergent surface energies from slab calculations, J. Phys. Condens. Matter 8 (36) (1996) 6525.
[51] L. Vitos, A.V. Ruban, H.L. Skriver, J. Kollar, The surface energy of metals, Surf. Sci. 411 (1) (1998) 186–202.
[52] Y. Tao, G. Ke, Y. Xie, Y. Chen, S. Shi, H. Guo, Adhesion strength and nucleation thermodynamics of four metals (Al, Cu, Ti, Zr) on AlN substrates, Appl. Surf. Sci. 357 (2015) 8–13.
[53] H.S. Abdelkader, H.I. Faraoun, Ab initio investigation of Al/Mo 2 B interfacial adhesion, Comput. Mater. Sci. 50 (3) (2011) 880–885.
[54] D.F. Johnson, E.A. Carter, Bonding and adhesion at the SiC/Fe interface, J. Phys. Chem. A 113 (16) (2009) 4367–4373.
[55] S. Lu, Q.M. Hu, R. Yang, B. Johansson, L. Vitos, First-principles determination of the $\alpha - \alpha'$ interfacial energy in Fe-Cr alloys, Phys. Rev. B 82 (19) (2010) 195103.
[56] S.J. Lee, Y.K. Lee, A. Soon, The austenite/ε martensite interface: a first-principles investigation of the fcc, Fe(111)/hcp, Fe(0001) system, Appl. Surf. Sci. 258 (24) (2012) 9977–9981.